A Simplified Ocean Physics? Revisiting Abyssal Recipes

CARL WUNSCH[a,b]

[a] *Harvard University, Cambridge, Massachusetts*
[b] *Massachusetts Institute of Technology, Cambridge, Massachusetts*

(Manuscript received 6 November 2022, in final form 21 February 2023, accepted 23 February 2023)

ABSTRACT: Simplified descriptions of the ocean are useful both for formulating explanatory theories and for conveying meaningful global attributes. Here, using a 26-yr average of a global state estimate from ECCO, the basis for Munk's "abyssal recipes" is evaluated on a global scale between 1000- and 3000-m depth. The two specific hydrographic stations he used prove untypical, with potential temperature and salinity more generally displaying different vertical scale heights, and thus differing in one-dimensional (in the vertical) values of mixing coefficients and/or vertical velocities. The simplest explanation is that the circulation is fully three-dimensional with temperature and salinity fields not describable with a one-dimensional steady balance. In contrast, the potential density and buoyancy are quantitatively describable through a one-dimensional exponential balance, and which calls for an explanation in terms of turbulent mixing processes.

KEYWORDS: Diapycnal mixing; Large-scale motions; Ocean circulation; Ocean dynamics

1. Introduction

Simplified descriptions of the large-scale ocean circulation and its stratification have led oceanographers to useful theoretical models. Those models include geostrophic balance (the thermal wind equations), Sverdrup balance, gyres, abyssal recipes, Stommel–Arons flows, etc. Some schematics (e.g., Talley 2013) call for possible equally simple explanation. While some of these constructs are powerful descriptors of the deep ocean as a whole (geostrophic balance), others are best understood as theoretical depictions of a physics that may apply locally (e.g., Ekman dynamics) or as schematics of physics that may well operate in partial domains (e.g., western boundary currents).

In recent years, with global observations available (altimeter, gravity, and scatterometer satellites, Argo, CTD sections), it has become clear that the ocean has a strong regional physics (e.g., Sonnewald et al. 2019) commonly dominated by the turbulence expected of such a large Reynolds number fluid (see Stommel 1948). Most of the theoretical descriptors have been based primarily upon the assumption of a steady-state ocean—a concept, when applied to instantaneous measurements such as a CTD cast, that is at least superficially at odds with the modern data. An earlier paper (Wunsch 2011) using a 16-yr duration circulation estimate from the Estimating Ocean Circulation and Climate Project (ECCO; see Wunsch and Heimbach 2007; Forget et al. 2015; Fukumori et al. 2019) average, sought to determine the quantitative applicability of conventional Sverdrup balance in a time-averaged state estimate—with spatially complex results [see Chen et al. (2022) for a time-dependent example]. A somewhat bleak prospect arises that, given the complicated boundaries, abyssal topography, spatial dependences of wind curl, and heat and moisture exchanges, etc., every point in the ocean will have a physics and kinematics distinct from that even a short distance away, describable only by difficult-to-understand high space- and time-resolution models. The appeal of simplified descriptions of the physics and kinematics of the general circulation is manifested, for example, in the widespread, misleading, cartoon of an ocean "conveyor."

The utility of many simplified descriptions is hardly in doubt, but it then becomes important to evaluate the extent to which the system can be quantitatively so described. In recent years, because of its importance in allied fields, the nature of the ocean circulation has attracted greatly increased interest from scientists who are often not experts in ocean observations and fluid-dynamics-based theory. Those fields include meteorology, climate and paleoclimate, biological structures, and others.

It is thus ever more important that the applicability of schematic simplifications of the global circulation should be made quantitatively plain. A particular example of a well-known and widely used simplification is studied here: the "abyssal recipes" paper of Munk (1966, hereafter M66).[1] Its applicability to a time-averaged observed and dynamically consistent ocean is considered. Results described below can be summarized as showing that the M66 results—in their original form—are *not* supported on a global basis. Consistency of the M66 results with the chosen pair of hydrographic station measurements of temperature and salinity appears to be the result either of great good fortune, or of personal acumen. A simple inference is, unsurprisingly, that the ocean must be treated as having at least a two-dimensional and most likely a full three-dimensional fluid flow structure and turbulent mixing. A different form of recipe is found—that the deep potential density/buoyancy field is almost everywhere well described by a simple exponential, a result needing explanation in terms of the now-known inhomogeneities in the vertical and horizontal of oceanic mixing by turbulence.

Denotes content that is immediately available upon publication as open access.

Corresponding author: Carl Wunsch, carl.wunsch@gmail.com

[1] Citations in Google Scholar number ≈1700.

DOI: 10.1175/JPO-D-22-0229.1

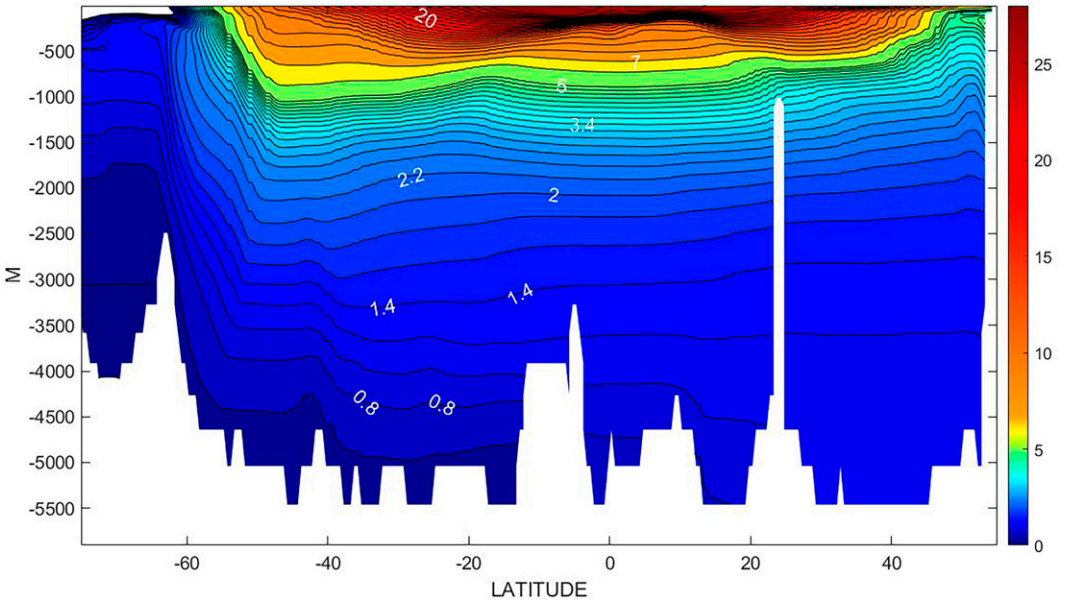

FIG. 1. Potential temperature along 165°W in the central Pacific Ocean from the 26-yr ECCO estimate average. Compare to line P15 in the WOCE Atlas. Topography is much smoother than exists in nature.

2. Abyssal recipes

M66 assumed a one-dimensional steady-state ocean in the "abyss." The attraction of the one-dimensional physics is plain, and it has been a useful strawman for discussions of oceanic mixing (e.g., Peterson and Callies 2022; Miller et al. 2020). Munk's paper is a tour-de-force: he successfully fit a simple exponential in the vertical coordinate z to the potential temperature (surface reference pressure), salinity, and a number of passive tracer concentrations, at two instantaneous hydrographic stations, and interpreted the abyssal physics generally. (He was careful to restrict the calculation to the depth interval above $z_1 = -4000$ m and below $z_2 = -1000$ m—a restriction subsequently widely ignored.) That the same scale heights well described potential temperature (T), salinity (S), and radiocarbon (^{14}C), made the results particularly convincing. The paper is a fecund discussion of the physics of oceanic mixing, including that at boundaries, by biology, instabilities, double diffusion, and more—along with a long list of sensible caveats.

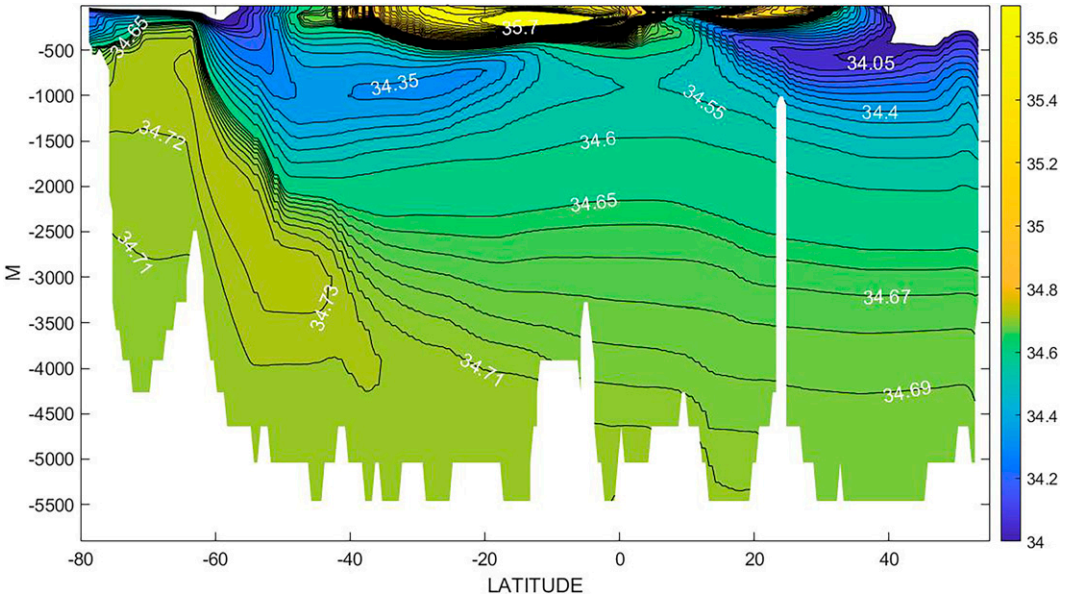

FIG. 2. 26-yr time-average salinity field along meridian 165°W from ECCO results. Compare to WOCE line P15. Here, and in other figures, colors saturate at the extremes.

Munk's physics was encompassed in the one-dimensional steady state of a tracer C as

$$w\frac{dC}{dz} - \kappa\frac{d^2C}{dz^2} = F, \quad \text{or} \tag{1a}$$

$$\frac{w}{\kappa}\frac{dC}{dz} - \frac{d^2C}{dz^2} = F/\kappa \tag{1b}$$

with $F = 0$ for interior temperature and salinity. Here w is a steady, constant, vertical velocity, and κ is a constant vertical diffusion coefficient. With $F = 0$, a general solution for a tracer C is,

$$C(z, t) = A_C + B_C \exp(z/h_C) + \varepsilon(z, t),$$
$$h_{T,S} = \kappa_{T,S}/w_{T,S} \quad z_1 \le z \le z_2 \tag{2}$$

for T and S separately, subject to their respective pair of boundary conditions. The term $\varepsilon(z, t)$ is a noise residual that would appear only in the observations—albeit at one time—not in the solution to Eq. (1a). The variable T is understood to be the potential temperature relative to the surface pressure. The solutions to Eq. (1a) for T, S, or their vertical derivatives, depend upon the boundary conditions imposed at depths z_1, z_2. If flux conditions, $F_B(z_i) = wC(z_i) - k\partial C(z_i)/\partial z$ are used, they must be identical at the two depths to maintain a steady state. With observations of T, S, concentration values on the two boundaries are perhaps more natural. In any case, an exponential structure within $z_1 \le z \le z_2$ does *not* depend upon the boundary values. An important point is that the same values of the scale height h_C can be consistent with both a temperature decreasing and salinity increasing with depth—depending upon the values and signs of A_C, B_C. Evidently, the recipe will fail if the vertical derivative changes sign *within* $z_1 \le z \le z_2$.

Munk's chosen data for T, S, produced consistent estimates of the scale height,

$$h_{T,S} = \frac{\kappa}{w}, \tag{3}$$

of about 0.8 km at both locations—consistent also with a linear T–S relation. Both fields displayed a very similar exponential decay with depth. A steady state was justified by referring to the small difference seen in two hydrographic stations two decades apart in the Mindanao Deep. Does such a balance work, quantitatively, globally for a time-average circulation?

Unless $\kappa_T \neq \kappa_S$, which is difficult to conceive in mechanically controlled one-dimensional turbulent mixing, separate estimation of κ, w depends upon the use of tracers satisfying a different equation, with $F \neq 0$, in Eq. (1a). Munk used ^{14}C, with a decay term, as well as oxygen with sources/sinks, and radon. Alternatively, an assumption of a constant global w can be made, based upon rough knowledge of the overall production of bottom waters necessarily upwelling back to the surface. The latter approach seemed consistent with the Stommel and Arons (1960) hypothesis of laterally uniform upwelling of bottom water. Overall, Munk found $\kappa \approx 10^{-4}$ m^2 s^{-1}, with $w \approx 1.2$ cm day^{-1} = 1.4×10^{-7} m s^{-1}. That all three estimated values of h_C were almost identical, and that the profiles of temperature and salinity had very similar decreases with depth, made the M66 conclusions very convincing.

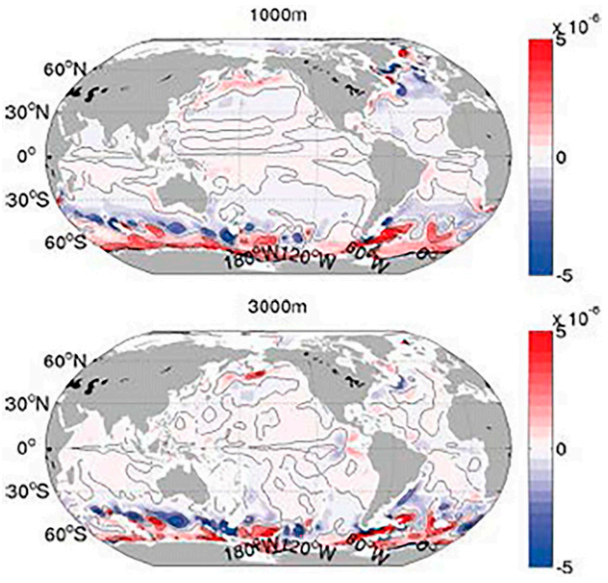

FIG. 3. Time-mean vertical velocity w (m s^{-1}) at two depths, from an ECCO state estimate (Liang et al. 2017). The relatively small scales appearing in the Southern Ocean and high northern latitudes are notable, along with the much larger-scale features at midlatitudes, particularly the zonality visible at 1000 m.

In the intervening decades, apart from the inference of a high degree of temporal and spatial variability in the circulation including intense geostrophically balanced eddies, numerous attempts to measure κ at middepths in the open ocean (e.g., Waterhouse et al. 2014; Gregg 2021; Moum 2021) have led, at these depths, generally to much lower estimates of κ—closer to 10^{-5} m^2 s^{-1}. Furthermore, the inference that most vertical (or diapycnal) mixing takes place at the boundaries including, especially, abyssal topographic features (e.g., Ferrari et al. 2016) are inconsistent with the original recipe, although already described as a possibility in M66. In retrospect, it is also puzzling that density-active tracers such as T or S would have the same physics as a passive tracer such as ^{14}C.

Overall (full depth ocean) boundary conditions in the vertical for temperature and salinity differ considerably—raising the question (e.g., Wunsch 2002) as to whether a single "thermohaline circulation" could possibly exist. Note too, that the first systematic abyssal measurements of the Pacific Ocean were not made until after M66 was written (Stommel et al. 1973; Kenyon 1983) and at the traditional coarse (non-eddy resolving) spatial resolution. Much later, Munk and Wunsch (1998) reinterpreted the abyssal recipes as applying only to basin or global horizontal integrals, ones that would encompass the boundary mixing processes.

Is the point-wise Eq. (1a) supported by direct observation? As already noted, strictly speaking, equations such as Eq. (1a) apply to a steady-state ocean. M66 worked in the geometrical coordinate z, a practice followed here, in recognition that the ECCO model employed below, is written in geometrical

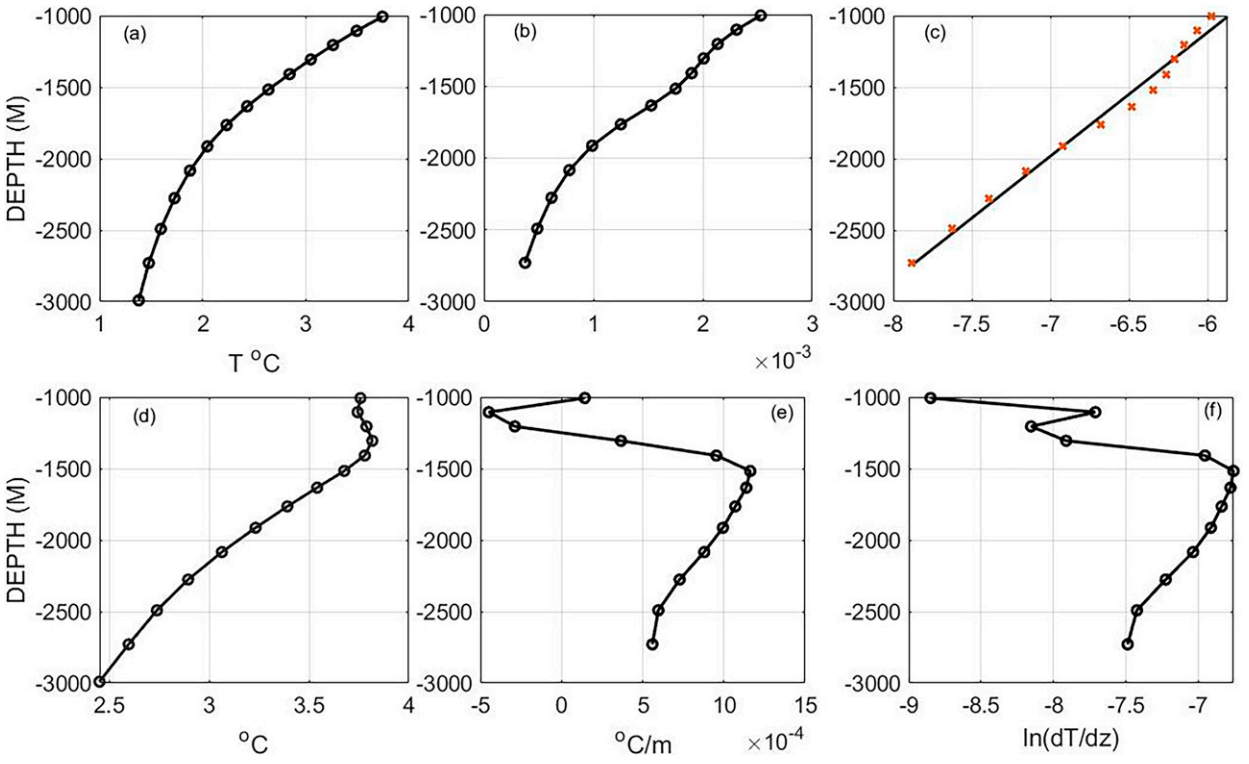

FIG. 4. (a) A temperature profile, (b) its derivative, and (c) the logarithm (base *e*) of the derivative for a position at 31°N, 127°W. Values fitted to the logarithm correspond to the points. The result is typical of regions where the exponential is a good, but not perfect, fit. (d)–(f) As in (a)–(c), but for a profile on the western side of the South Atlantic at 17°S, 25°W and no fit is shown in (d)—where the sign reversal in the derivative is clear. There the fit to the temperature derivative is rejected; compare WOCE section A08.

coordinates. A strong argument can be made that an isopycnal or neutral density coordinate should be used—particularly in near-boundary regions where the isopycnals differ substantially from the horizontal. Isopycnal depths are a product of the estimate itself, and their use as a coordinate system potentially introduces added complexity into the understanding of the accuracy of the results. None of the overall qualitative conclusions concerning the *open ocean* here appear dependent upon which vertical coordinate is used, although small quantitative differences would necessarily occur.

The ECCO state estimate has made possible a 26-yr average of the ocean circulation from a free-running model constrained within estimated uncertainties to a great variety of global-scale datasets (Argo, altimetry, CTDs, surface flows, meteorological fields, etc.). That estimate has the virtue of satisfying all of the conventional physical conservation rules over the 26 years, including energy, mass, vorticity, salt, etc., in contrast to most "reanalyses" (see, e.g., Bengtsson et al. 2004). Conservation is satisfied in the sense that changes in energy, etc., can all be attributed to specific forcing or dissipation. Hautala and Finucane (2022) provide a useful discussion of the extent to which dominant abyssal long-wavelength features in individual transoceanic sections are nearly time independent—an axiom of hydrographic oceanography since its very beginning. No claims are made here about results from significantly longer averaging periods—with known overall global baroclinic adjustment times extending to thousands of years and the disequilibrium of the modern-day circulation. Fields from quasi-synoptic data will be intrinsically noisy compared to the estimated time-average fields, the former showing eddy, internal wave and other time-dependent noise.

The time average as used is on a grid of 1° in longitude, and 1/2° in latitude. Any model, such as the one used here, without extremely high resolution, will not resolve the intricate boundary layers present at all boundaries, including those at the sea surface, on the complex bottom topography, and on coastal sidewalls. To the extent that the interior fields do generally replicate within error estimates the various global datasets, as is true here, near-boundary values will be adjusted so that the unresolved structure is consistent with the interior in what is a form of inverse problem for determining effective boundary conditions from the interior solution. An example is the Gulf Stream, which is not dynamically resolved. But within the ECCO estimates, its relatively crude representation will nonetheless carry the volume, heat, etc. transports necessary for consistency with the constrained calculated interior values. Discussion below excludes the Arctic regions which require special treatment (Nguyen et al. 2021).

The original recipe was based upon the assumption that the exponential fit to both temperature and salinity (and tracers) vertical structures would produce the same scale height at common locations and with an overall vertical dependence through a common turbulent mixing process.

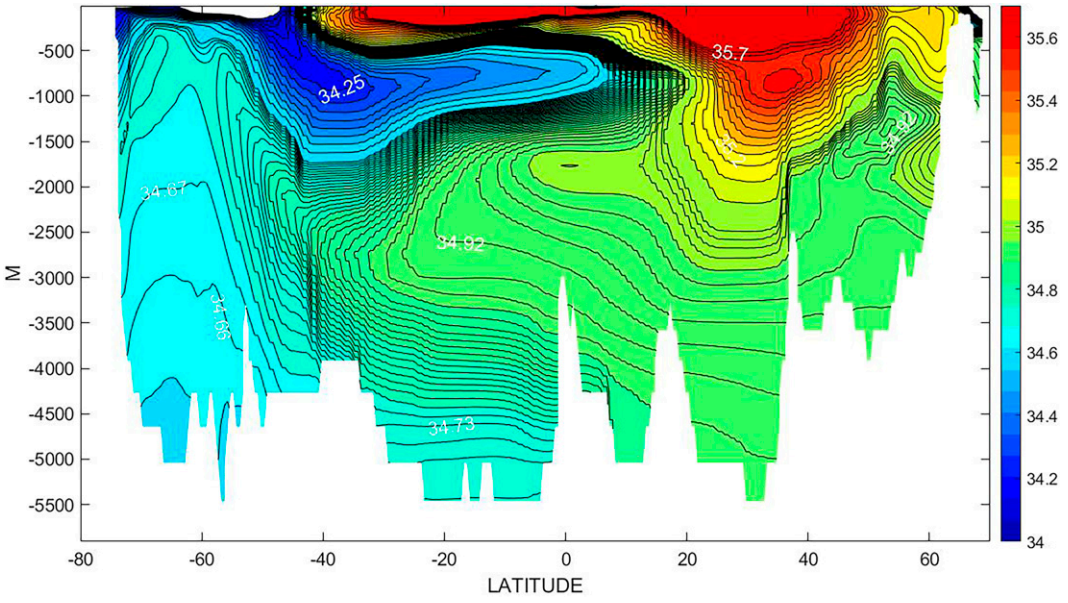

FIG. 5. ECCO mean salinity along the 30°W section in the Atlantic Ocean displaying the complex structure there. Compare WOCE section A08. The corresponding temperature section (not shown) has a comparable structure to compensate the density field so as to render it everywhere stable.

Figures 1 and 2 display the ECCO version 4, release 4 (v4r4) estimated average potential temperature and salinity along the 165°W Pacific meridian. On the large scale, as expected, there is good agreement with the WOCE Atlas quasi-synoptic section (P15) near this meridian. (Readers of this paper will find it useful to have available the WOCE electronic Atlas plates: http://woceatlas.ucsd.edu/.) Agreement is expected because the WOCE section data are included in the ECCO least squares fit within their estimated noise and errors. ECCO estimates are naturally much smoother than the quasi-synoptic sections. A one-dimensional dependence in any of these fields is not obvious.

An immediate difficulty with M66 arises visually in both the ECCO and nearby WOCE versions of the section: in contrast with potential temperature, salinity generally increases with depth at all latitudes below about 1–2 km, contrary to the particular M66 pair of stations data. The central Pacific is often regarded as the simplest part of the global ocean, but identical vertical profiles in T and S are not consistent with the estimate in either the WOCE data or the ECCO estimate, although T and S can nonetheless have the same value of h_C.

Liang et al. (2017) found, in a discussion of the time-mean vertical velocity w of the ECCO estimate, including

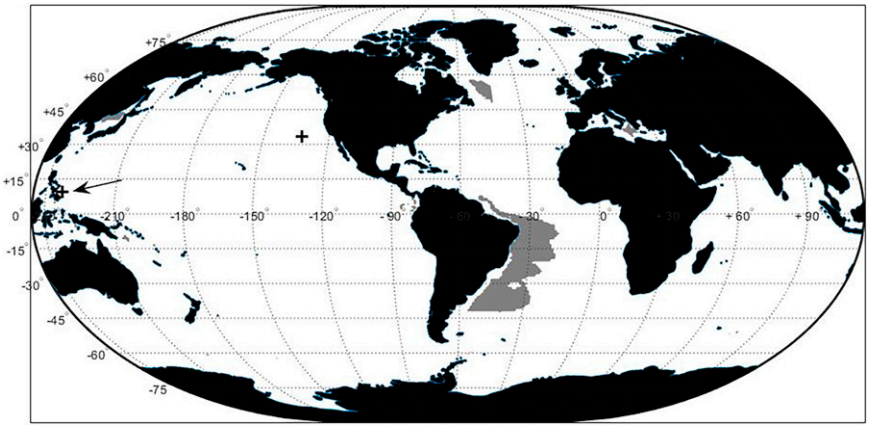

FIG. 6. The gray area shows the regions where potential temperature changes sign within the range $-3000 \le z \le -1000$. Note the small area in the northwest North Atlantic also having a sign change. Here and elsewhere, positions of the two M66 hydrographic stations are indicated by "+," one of them adjacent to the Philippine archipelago.

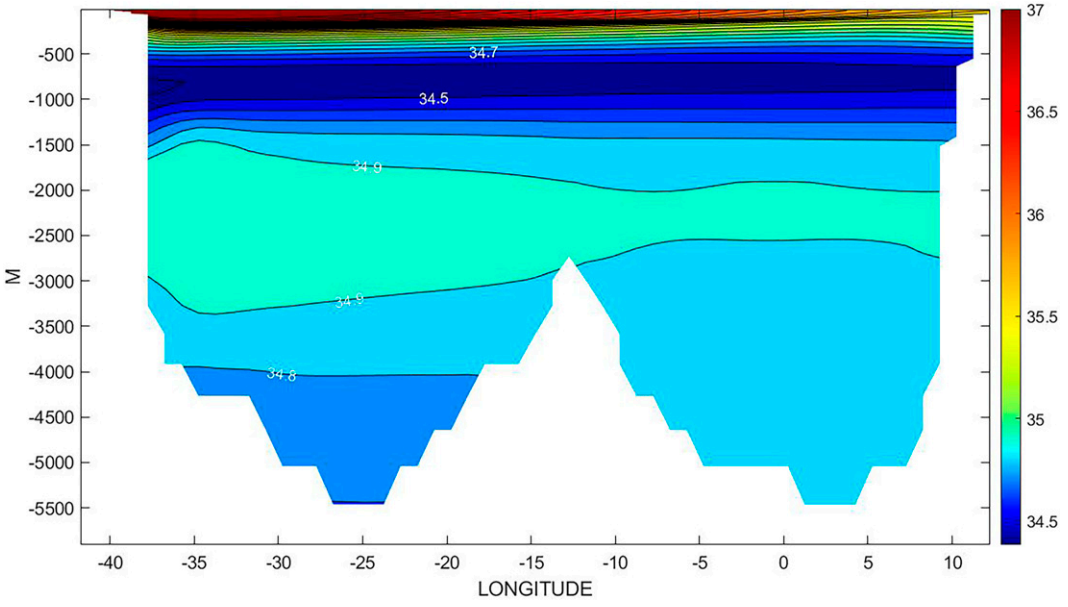

FIG. 7. ECCO mean salinity at 19°S as a 26-yr average. Note the middepth maximum, particularly on the west.

that from the residual mean flow, that it has a complex spatial variability, varying in sign, even in the North Pacific; see Fig. 3. The extent to which a one-dimensional balance can be said to represent the observed ocean is now pursued. Positions of the two M66 hydrographic profiles are shown as "+" in the mapped fields below (Fig. 6 and subsequently). They lie close to boundaries on the eastern and western sides of the North Pacific.

In proceeding, Eq. (2) can be used directly in a nonlinear least squares fit to the ECCO time-average at each lateral position. Such a result (not shown) was computed using a trust algorithm as packaged by MATLAB. However, in the interest of obtaining some simple guidance as to the uncertainty of the parameters, a fit was made instead to $\ln(dC/dz)$, in which the vertical derivative suppresses the constant A_C in Eq. (2) and the logarithm renders the least

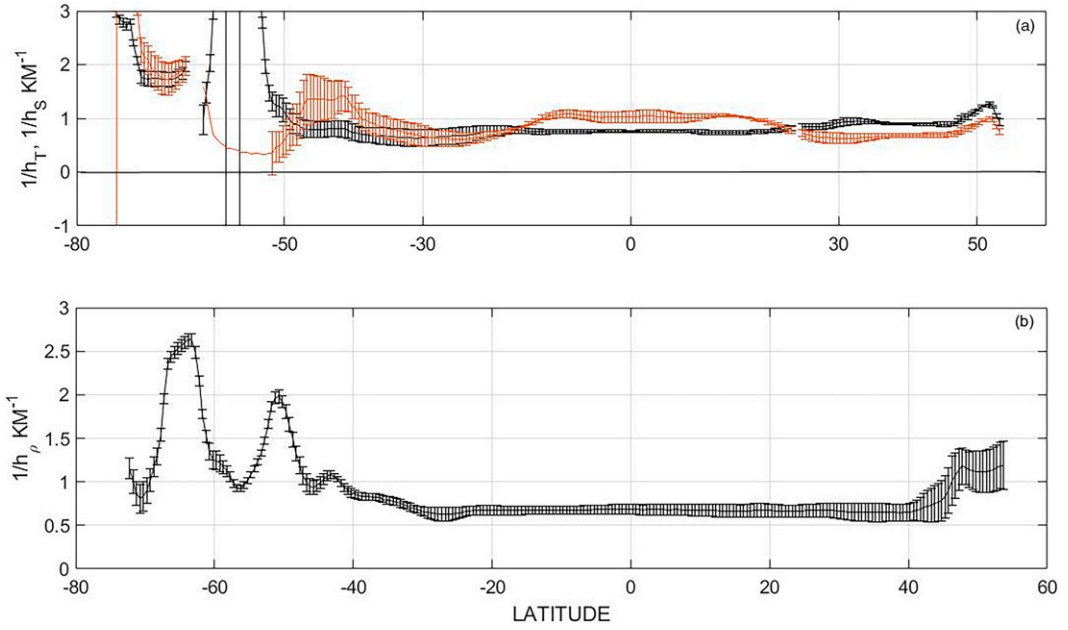

FIG. 8. (a) $1/h_T$ (black) and $1/h_S$ (red) in the mid-Pacific Ocean along a longitude 165°W with the scatter of the fit. A small band of overlapping values exists near 30°S. (b) $1/h_\rho$ along 20°W in the Atlantic.

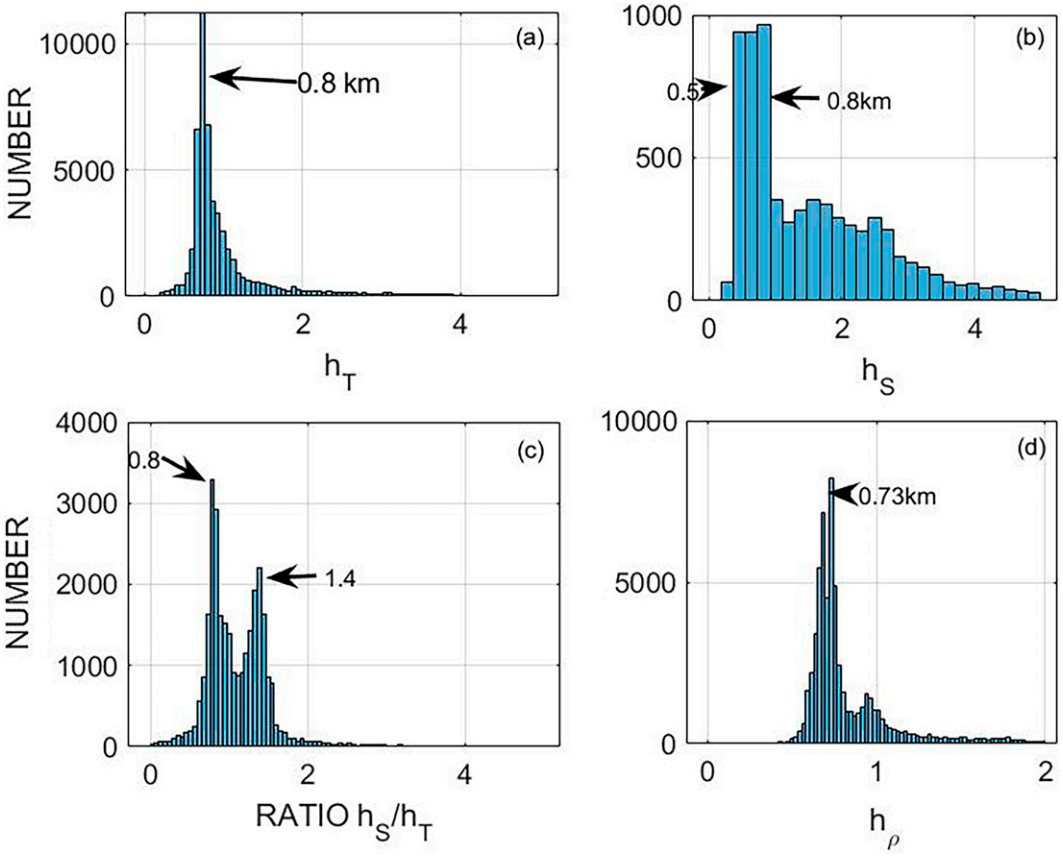

FIG. 9. (a) Histogram of the values of h_T. The largest number occurs near 0.8 km—remarkably close to the M66 value. (b) Values of h_S. (c) Distribution of the ratio, h_S/h_T. (d) Values of h_ρ.

squares problem linear in $1/h_C$. That approach has the disadvantage of requiring a vertical derivative of the ECCO estimate, but provides a straightforward formal estimate of the variance of $1/h_C$ from the scatter of the residual in the conventional linear least squares solution (e.g., Wunsch 2006).

Attention is now restricted to the range $z_1 = -3000$ m, $z_2 = -1000$ m, thus avoiding encounters with the large-scale midocean

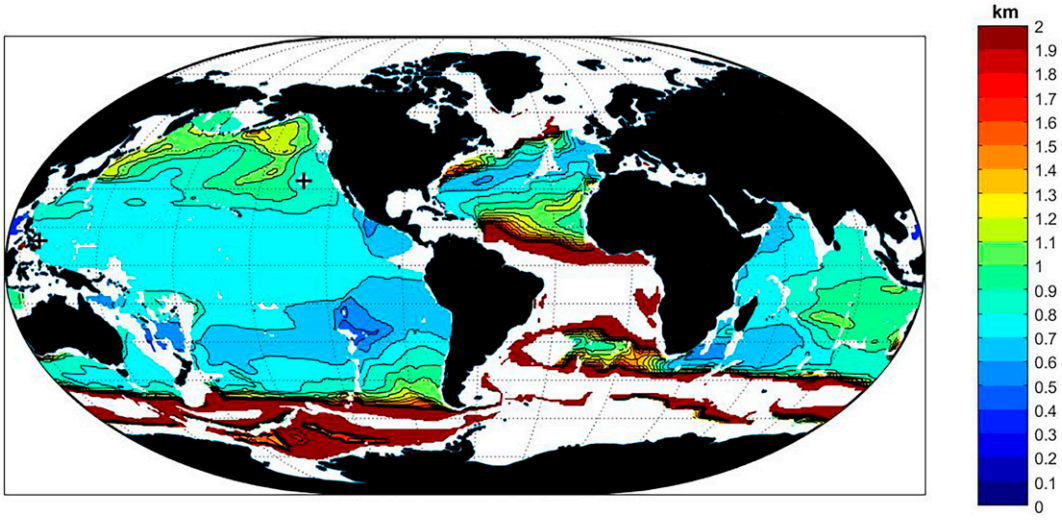

FIG. 10. h_T where $1/h_T$ formally differs from zero within the scatter. Color saturates at 2 km. Blank areas are either too shallow, or a sign change occurs in the vertical derivative, or the computed value leaves a large residual. Much of the Southern Ocean and the South Atlantic fail to meet the criteria set.

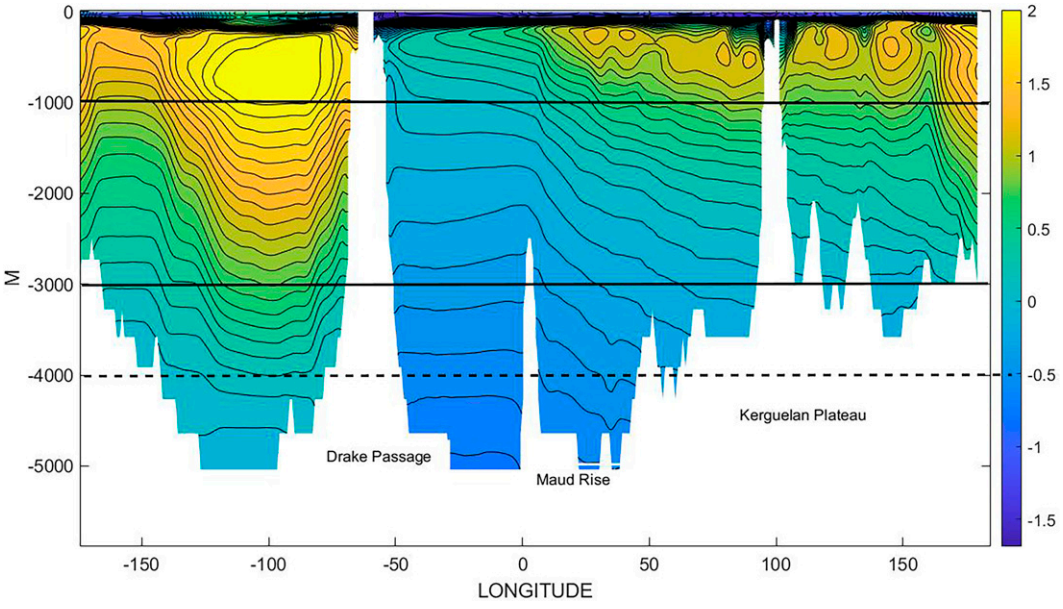

FIG. 11. Potential temperature in the time-averaged ECCO section at 64°S in the Southern Ocean. The complex zonal structure is apparent, as is the region of relatively steep zonal gradients at depth. Unusually in the global ocean, topographic disturbances are visible over the whole water column. Horizontal lines mark the depth ranges of the analyses in this paper. Connections between these structures, their density equivalents, and those in the interior ocean are the subject of much speculation in the literature.

ridges. This depth range is depicted in the model by 14 layers. (A brief discussion of the results from using $z_1 = -4000$ m can be seen in the appendix.)

Residuals are found at only 13 depth values and should *not* be assumed to have a Gaussian distribution. The formal variance of the solution will thus be referred to here as the "scatter" and denoted σ_C^2.

3. Temperature recipe

Figure 4 shows a profile not untypical of the central North Pacific, including its vertical derivative, the logarithm of the derivative, and the best fit to the logarithm. In contrast, the same figure shows the profile results from a South Atlantic position, and for which the results are rejected outright, because $\partial T/\partial z$ changes sign within the given depth range. [See the meridional ECCO salinity section down 20°W in Fig. 5 and compare to the WOCE sections A16, A08 in the Atlantic Atlas or the plates in Wefer et al. (1996).] Figure 6 for the global ocean displays the region of the South Atlantic near the South American coast where a temperature derivative sign change occurs in the depth interval being examined. This region is one with an intense southward-going deep western boundary current carrying substantial amounts of salt-heavy, relatively warm, North Atlantic Deep Water that, in addition, dominates the interior at depth. Other profiles (not shown) are rejected on

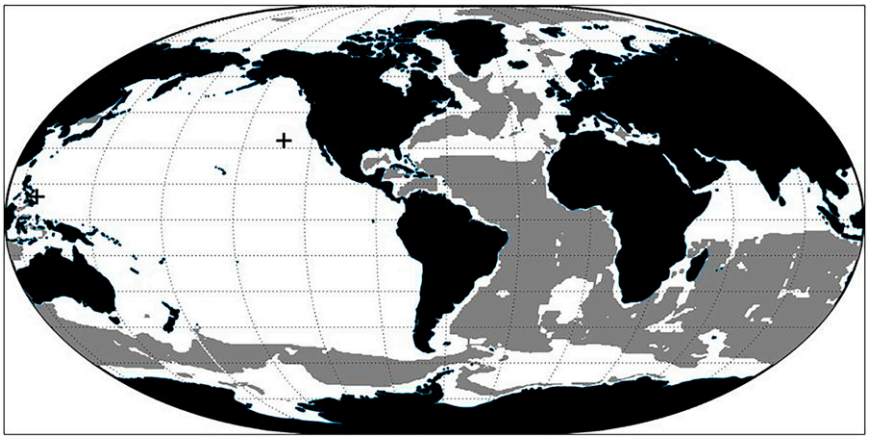

FIG. 12. Gray is the region of salinity derivative reversal within the depth range of 1–3 km.

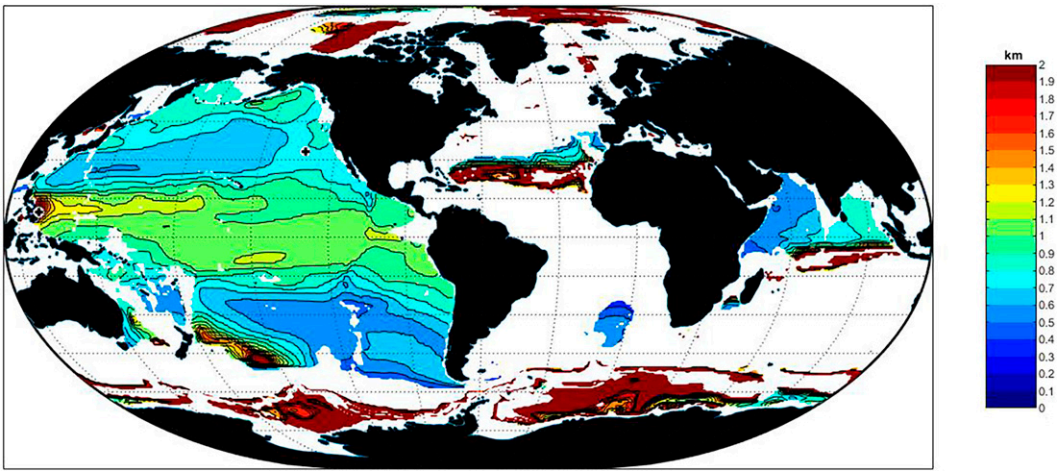

FIG. 13. Significant values of the salinity scale height (km). Color saturates at 2 km.

the basis of producing a poor fit, even if the derivative is of one sign. The criterion for acceptance is that the fit has to account for at least 80% of the formal variance in the profile. A zonal salinity section at 19°S, with a middepth maximum across the entire basin is visible in Fig. 7 and again compensated in density by a corresponding temperature maximum.

In the global fit, water depths less than 3000 m are thus excluded, as are values where the scatter in $(1/h_T)$ included zero. The results for the reciprocal scale heights along 165°W in the ECCO average are shown in Fig. 8 along with the formal one standard deviation from the scatter.

The fit is a poor one near 60°S and the values are rejected. In the middle range of latitudes, between about 55°S and 55°N, values are almost all formally different from zero. High-latitude values in both hemispheres produce poor fits.

The near-global distribution of values of h_T appears in Fig. 9. Munk's value from extremely limited data is remarkably close, globally, to the most common value. A map of h_T is shown in Fig. 10 with values greater than 2 km lumped together. Blank regions are areas where the uncertainty in $1/h_T$ rendered the result consistent with zero within a $2\sigma_T$ scatter, or the water depth was less than 3000 m. Major topographic features do not produce any obvious structure, with the possible exception of a region in the South Pacific over the east Pacific rise and in the Southern Ocean. Some very rough correspondences—visible by eye—with the low eddy-energy maps of Wunsch and Stammer (1995), the spectral slope regions of Xu and Fu (2012), and with the regional barotropic physics maps of Sonnewald et al. (2019) exist. These and other elements may well underlie an eventual rationalization of the scale height distributions.

Large areas of misfit, or of scale heights greater than 2 km are apparent. The complex thermal (and by implication salinity) field in the Southern Ocean at 64°S can be seen in Fig. 11. Unlike most of the rest of the World Ocean, bottom topography disturbances appear to occupy much of the water

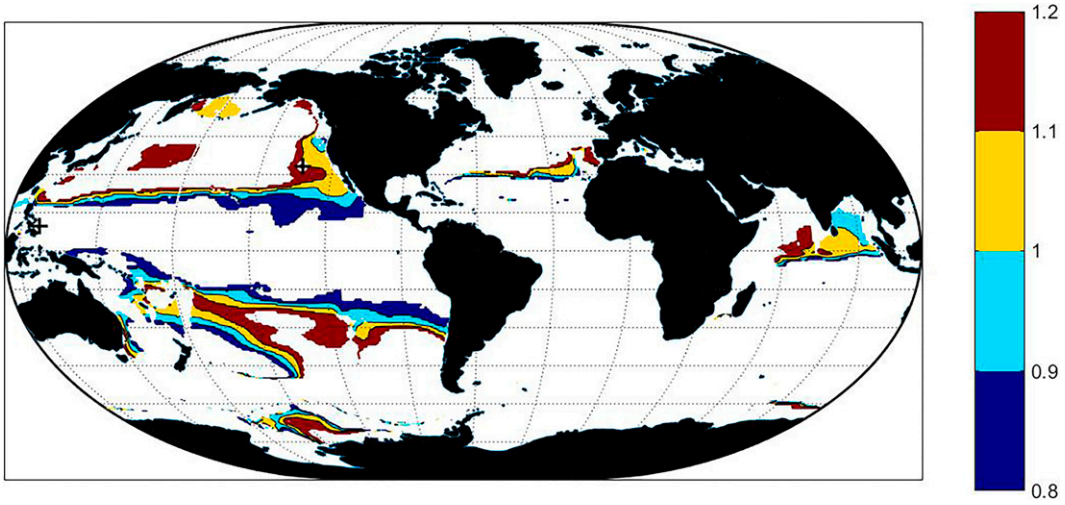

FIG. 14. Colored shading shows where the ratio h_S/h_T lies within 0.8–1.2. The M66 eastern mooring result falls within this range.

column. A number of theoretical analyses (e.g., Wolfe and Cessi 2010; Miller et al. 2020, and references there) imply that in the global, ocean stratification is set by the structures in the Southern Ocean. The density field is discussed briefly below, but no attempt is made here to rationalize the physics of the varying structures in the abyssal temperature distribution.

If a one-dimensional fit is insisted upon, let $r(z) = w(z)/\kappa(z)$, $F = 0$, and defining,

$$T(z) = \exp\left[-\frac{1}{2}\int r(z)dz\right]\hat{T}(z),$$
$$\frac{d^2T}{dz^2} - \left[\frac{1}{4}r(z)^2 + \frac{1}{2}\frac{dr}{dz}\right]\hat{T}(z) = 0, \quad (4)$$

(Whittaker and Watson 1927, p. 194) and $r(z)$ could be chosen by an appropriate fit. But then the attractive simplicity of the abyssal recipe is lost.

4. Salinity recipe

The salinity field S was treated identically to that of temperature. Figure 12 shows the much more extended area in which $\partial S/\partial z$ changes sign between z_1 and z_2. In the South Atlantic, overlap exists with the much smaller inversion region for temperature. Most of the Atlantic, the southern half of the Indian Ocean, and of the Southern Ocean are necessarily excluded. The fit with scatter along 165°W is shown in Fig. 8a. (A reviewer has raised the question of why the extended region of salinity reversal in the North Atlantic does not also have a corresponding temperature reversal? Examination of the ECCO sections or of the WOCE Atlas plates shows that regions of temperature reversal there are either above 1000 m in the Mediterranean Water and/or confined to laterally small, unresolved, areas.)

With excluded values not used, Fig. 9b shows the distribution of values of h_S, one having a long tail. Distribution of the ratio h_S/h_T is in Fig. 9c and values of h_S both larger and smaller than h_T exist.

Figure 13 displays h_S using the same criterion as for temperature and Fig. 14 shows the global distribution of the ratio h_T/h_S that lies in the range from 0.8 to 1.2, that is, within about 20%. The region (Fig. 14) where the two scale heights agree within ±20% occupies a very small region of ocean. That the original recipes implied agreement of the scale heights globally is a description which must be rejected. Much of the ocean, however, outside the Atlantic and Southern Oceans, has T and S fields that can be described separately as exponential—a useful result in itself. One should not, however, infer that one-dimensional physics dominates.

5. Radiocarbon (^{14}C)

To determine k, w separately an equation differing from Eq. (1a) with $F = 0$ must be used. M66 discussed a number of spatially dependent fields including oxygen (cf. Wyrtki 1962), radon, etc., but focused primarily upon the values $\Delta^{14}C = {}^{14}C/{}^{12}C$, that is, the ratio of the concentrations of two isotopes of carbon. Results appeared consistent with the values of w, k stated above. Craig (1969) strongly criticized Munk's use of $\Delta^{14}C$ in Eq. (1a) with $F = -\lambda C$, as it was treating what is a ratio of concentrations as though only the numerator varied spatially, and ignoring the complex source/sink contributions within the water column. He went on to the conclusion that in M66 those two errors fortuitously cancelled each other, because doing it "right," Craig obtained essentially the same numerical values as M66. One might add to the issues the assumption of a steady-state distribution of $\Delta^{14}C$, neglecting the anthropogenic $^{14}C(t)$ transient over decades.

Carbon-14 is an example of a tracer commonly used to compute a water mass "age." with its own complex spatial structure. In that form, other modeling problems arise (e.g., Siberlin and Wunsch 2011) as well. With all of the issues surrounding its use, including a large amount of noise in the data, the radiocarbon distribution would not fit any simple recipe (see, e.g., Schlitzer 2007).

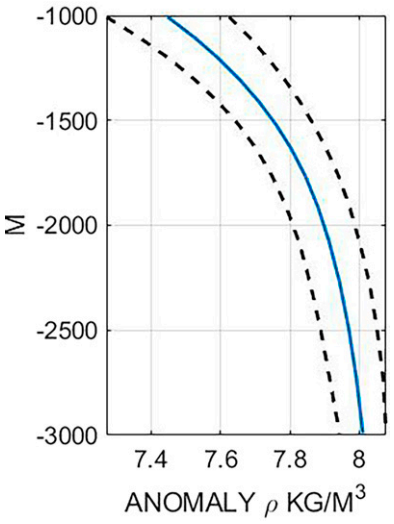

FIG. 15. The global mean potential density anomaly as a function of depth equatorward of 50° latitude along with the RMS scatter. The mean is that of the grid values, and which were not area weighted.

6. ρ recipe

That the abyssal recipes in their original form at any given position are not a very useful oceanic descriptive simplification is clear. The potential density field ρ, being a combination of temperature and salinity fields, is expected to be different, as turbulent mixing is anticipated to operate directly on ρ. Apart from the small effects of molecular double diffusion, turbulence does not act separately on T, S. Its behavior would be equivalent to that of the buoyancy, $g\rho(z) = G[T(z), S(z)]$, where g is local gravity, and G an equation of state. (Dependence on horizontal coordinates is implicit.) Consider $\Delta\rho$, the anomaly of the potential density in the ECCO average (Jackett et al. 2006; Forget et al. 2015) relative to surface pressure and with a similar exponential fit, as used above (the global horizontal mean and its scatter are shown in

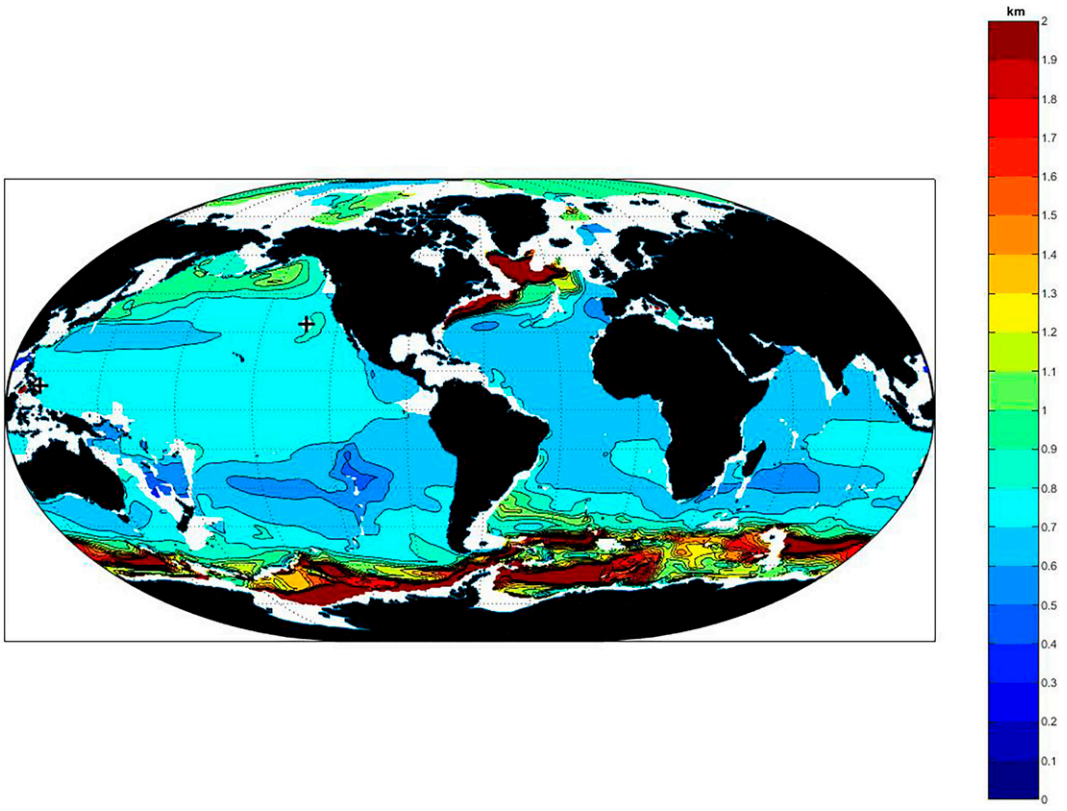

FIG. 16. Map of h_ρ. The Southern Ocean and the high-latitude North Atlantic Ocean and the region in the South Atlantic seen in temperature and salinity stand out in the ρ field from the bulk of the global ocean. Blank areas correspond to regions of poor fit (but no instances of unstable stratification are seen). Color saturates at 2 km.

Fig. 15). No reversals of the vertical derivative exist in the model domain (static stability is found everywhere in the time average). Figure 8b shows the estimated scale height along a meridional Atlantic section used above and where the T, S fits were rejected, but where a potential density fit is adequate. Once again, very large variations occur within the Southern Ocean; see Fig. 11. A histogram and a map of the scale height h_ρ are shown in Figs. 9d and 16.

The tendency to multimodality is not explained. Evidently, the exponential is a much more universal descriptor of the density field than for either T or S alone, but with a spatial variation that needs to be interpreted in terms of the regional and global physics.

That buoyancy/density is describable by a one-dimensional exponential curve is a useful, near-global, description, but an inference of a one-dimensional physics remains unjustified. The literature, some cited above, on the physics setting the buoyancy fields is now extensive (see Rogers et al. 2023, and references therein).

7. Discussion

In the search for general (global-scale) descriptions of the ocean, use of the original formulation (M66) of abyssal recipes is evidently a Procrustean procedure when applied to a global temporal average of oceanic temperature and salinity between 1- and 3-km depth (roughly one-half of the global oceanic volume). Munk and Wunsch (1998) did reinterpret it as a basin or global integral—for which the physical basis is clearer as it incorporates the major spatial variability. Regions where Eq. (1a) consistently applies to both temperature and salinity are very limited. M66, however, remains an important discussion of the general physics of oceanic mixing and the distribution of tracers.

The exponential profile *is* a useful descriptive fit to the potential density over most of the ocean and thus stands as a surviving, general circulation description.[2] Understanding the spatial structure and underlying physics of that result takes one away from the present search for a simple description into the details of oceanic turbulent mixing and its likely very strong two- and three-dimensional spatial structures (see, e.g., Yang and Tziperman 2022; Rogers et al. 2023, and references therein). Temperature and salinity fields evidently each require a three-dimensional balance for quantitative description—one requiring full specification of their boundary conditions.

The M66 inference about T, S profiles is seen to *not* be a generally useful ocean depiction. On the other hand, M66 is an excellent example of Munk's maxim that "Asking the right question is much more important than finding the right

[2] Invoking the Yiddish expression, one might call it "a bisl recipe."

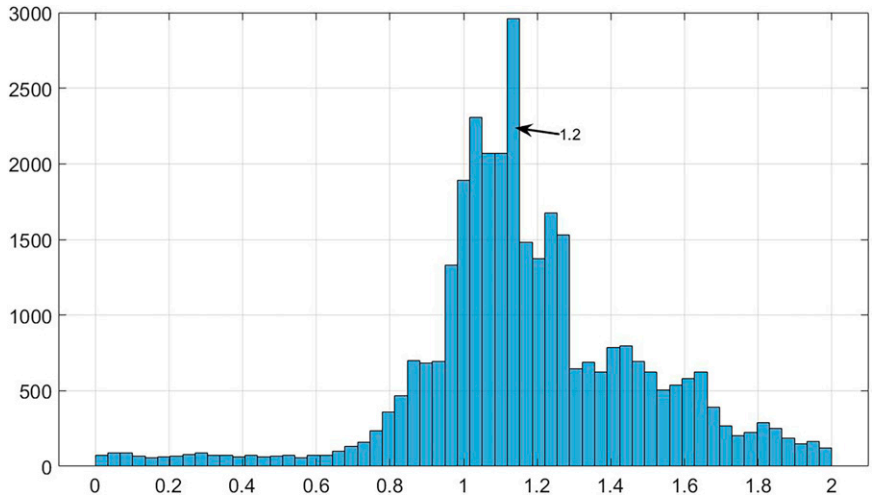

FIG. A1. Distribution of values for the ratio of the 4000-m range scale height to that of the 3000-m range. Small numbers of outlying values have been omitted.

answer," the paper having generated widespread, multidecadal, discussion of how the ocean does mix.

Remaining potentially simplifying ocean depictions of the mean state can be examined. Results such as those in Fig. 3 have long been known to show that the uniform Stommel/Arons vertical velocity does not appear in nature (albeit it too remains a powerful theoretical idea). Sverdrup balance does apply in some areas in the time average (Wunsch 2011). Other simplifying ideas, such as the Ekman and β spirals, will be described elsewhere.

Acknowledgments. All of the participants in the ECCO Project contributed to make this work possible. Thanks to Mason Rogers for discussion and help with the density field calculations. I'm grateful to the reviewers for very careful readings and comments. Supported in part by the Cecil and Ida Green Professorship at MIT.

Data availability statement. No observational data were used directly in this paper. The ECCO state estimate as well as the underlying model and the variety of data used for it can be found on the ECCO JPL/NASA websites: https://ecco.jpl.nasa.gov/drive/files/Version4/Release4.

APPENDIX

Temperature, $z_1 = -4000$ m

If the temperature depth range is extended to 4000 from 3000 m, the most common value is increased by about 10%

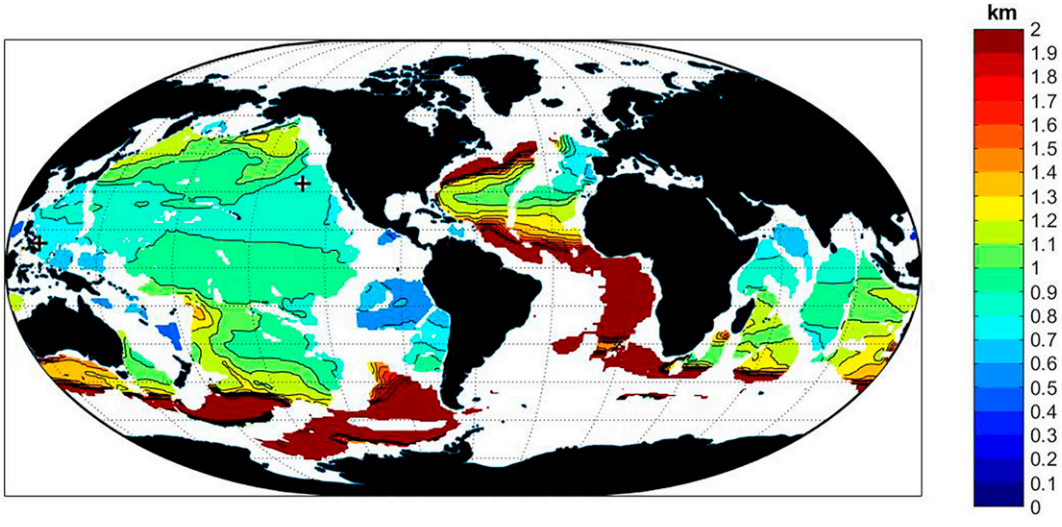

FIG. A2. Scale height map h_T (km) for significant fits over the range $-4000 \le z \le -1000$ m. Colors saturate at 0 and 2 km. In the blank areas, the fit has been rejected owing to a large scatter or reversal of the vertical derivative or for a depth limitation.

as seen for the ratio of the two estimates of h_T in Fig. A1. Values near 1 km are common, but many other values can differ radically. The overall pattern (Fig. A2) remains the same, but with large values of h_T now appearing in a more extensive area in the eastern South Atlantic. Midocean ridge shallow regions become visible in the blank areas. The M66 eastern Pacific hydrographic station produces a result now consistent with that in a quasi-zonal band across the entire ocean that includes the M66 eastern station, and nearly that for the western one.

REFERENCES

Bengtsson, L., S. Hagemann, and K. I. Hodges, 2004: Can climate trends be calculated from reanalysis data? *J. Geophys. Res.*, **109**, D11111, https://doi.org/10.1029/2004JD004536.

Chen, G., R. X. Huang, Q. Peng, and X. Chu, 2022: A time-dependent Sverdrup relation and its application to the Indian Ocean. *J. Phys. Oceanogr.*, **52**, 1233–1244, https://doi.org/10.1175/JPO-D-21-0223.1.

Craig, H., 1969: Abyssal carbon and radiocarbon in the Pacific. *J. Geophys. Res.*, **74**, 5491–5506, https://doi.org/10.1029/JC074i023p05491.

Ferrari, R., A. Mashayek, T. J. McDougall, M. Nikurashin, and J.-M. Campin, 2016: Turning ocean mixing upside down. *J. Phys. Oceanogr.*, **46**, 2239–2261, https://doi.org/10.1175/JPO-D-15-0244.1.

Forget, G., J.-M. Campin, P. Heimbach, C. Hill, R. Ponte, and C. Wunsch, 2015: ECCO version 4: An integrated framework for non-linear inverse modeling and global ocean state estimation. *Geosci. Model Dev.*, **8**, 3071–3104, https://doi.org/10.5194/gmd-8-3071-2015.

Fukumori, I., O. Wang, I. Fenty, G. Forget, P. Heimbach, and R. M. Ponte, 2019: ECCO Version 4 release 4. PO.DAAC, accessed 9 May 2023, https://ecco.jpl.nasa.gov/drive/files/Version4/Release4/doc/v4r4_synopsis.pdf.

Gregg, M. C., 2021: *Ocean Mixing*. Cambridge University Press, 378 pp.

Hautala, S. L., and G. Finucane, 2022: Persistence of the large-scale interior deep ocean circulation in global repeat hydrographic sections. *Geophys. Res. Lett.*, **49**, e2021GL097264, https://doi.org/10.1029/2021GL097264.

Jackett, D. R., T. J. McDougall, R. Feistel, D. G. Wright, and S. M. Griffies, 2006: Algorithms for density, potential temperature, conservative temperature, and the freezing temperature of sea water. *J. Atmos. Oceanic Technol.*, **23**, 1709–1728, https://doi.org/10.1175/JTECH1946.1.

Kenyon, K. E., 1983: Sections along 35°N in the Pacific. *Deep-Sea Res. A*, **30**, 349–369, https://doi.org/10.1016/0198-0149(83)90071-7.

Liang, X., M. Spall, and C. Wunsch, 2017: Global ocean vertical velocity from a dynamically consistent ocean state estimate. *J. Geophys. Res. Oceans*, **122**, 8208–8224, https://doi.org/10.1002/2017JC012985.

Miller, M. D., X. Q. Yang, and E. Tziperman, 2020: Reconciling the observed mid-depth exponential ocean stratification with weak interior mixing and Southern Ocean dynamics via boundary-intensified mixing. *Eur. Phys. J. Plus*, **135**, 375, https://doi.org/10.1140/epjp/s13360-020-00375-y.

Moum, J. N., 2021: Variations in ocean mixing from seconds to years. *Annu. Rev. Mar. Sci.*, **13**, 201–226, https://doi.org/10.1146/annurev-marine-031920-122846.

Munk, W., and C. Wunsch, 1998: Abyssal recipes II: Energetics of tidal and wind mixing. *Deep-Sea Res. I*, **45**, 1977–2010, https://doi.org/10.1016/S0967-0637(98)00070-3.

Munk, W. H., 1966: Abyssal recipes. *Deep-Sea Res. Oceanogr. Abstr.*, **13**, 707–730, https://doi.org/10.1016/0011-7471(66)90602-4.

Nguyen, A. T., H. Pillar, V. Ocaña, A. Bigdeli, T. A. Smith, and P. Heimbach, 2021: The Arctic subpolar gyre state estimate: Description and assessment of a data-constrained, dynamically consistent ocean-sea ice estimate for 2002–2017. *J. Adv. Model. Earth Syst.*, **13**, e2020MS002398, https://doi.org/10.1029/2020MS002398.

Peterson, H. G., and J. Callies, 2022: Rapid spinup and spindown of flow along slopes. *J. Phys. Oceanogr.*, **52**, 579–596, https://doi.org/10.1175/JPO-D-21-0173.1.

Rogers, M., R. Ferrari, and L. Nadeau, 2023: Middepth recipes. *J. Phys. Oceanogr.*, https://doi.org/10.1175/JPO-D-22-0225.1, in press.

Schlitzer, R., 2007: Assimilation of radiocarbon and chlorofluorocarbon data to constrain deep and bottom water transports in the world ocean. *J. Phys. Oceanogr.*, **37**, 259–276, https://doi.org/10.1175/JPO3011.1.

Siberlin, C., and C. Wunsch, 2011: Oceanic tracer and proxy time scales revisited. *Climate Past*, **7**, 27–39, https://doi.org/10.5194/cp-7-27-2011.

Sonnewald, M., C. Wunsch, and P. Heimbach, 2019: Unsupervised learning reveals geography of global ocean dynamical regions. *Earth Space Sci.*, **6**, 784–794, https://doi.org/10.1029/2018EA000519.

Stommel, H., 1948: Theoretical physical oceanography. Yale Scientific Magazine, 6–22.

——, and A. B. Arons, 1960: On the abyssal circulation of the world ocean—I. Stationary planetary flow patterns on a sphere. *Deep-Sea Res.*, **6**, 140–154, https://doi.org/10.1016/0146-6313(59)90065-6.

——, E. D. Stroup, J. L. Reid, and B. A. Warren, 1973: Transpacific hydrographic sections at Lats. 43°S and 28°S: The SCORPIO Expedition—I. Preface. *Deep-Sea Res. Oceanogr. Abstr.*, **20** (1), 1–7, https://doi.org/10.1016/0011-7471(73)90039-9.

Talley, L. D., 2013: Closure of the global overturning circulation through the Indian, Pacific, and Southern Oceans: Schematics and transports. *Oceanography*, **26**, 80–97, https://doi.org/10.5670/oceanog.2013.07.

Waterhouse, A. F., and Coauthors, 2014: Global patterns of diapycnal mixing from measurements of the turbulent dissipation rate. *J. Phys. Oceanogr.*, **44**, 1854–1872, https://doi.org/10.1175/JPO-D-13-0104.1.

Wefer, G., W. H. Berger, G. Siedler, and D. J. Webb, Eds., 1996: *The South Atlantic: Present and Past Circulation*. Springer, 644 pp.

Whittaker, E. T., and G. N. Watson, 1927: *A Course of Modern Analysis*. 4th ed. Cambridge University Press, 408 pp.

Wolfe, C. L., and P. Cessi, 2010: What sets the strength of the middepth stratification and overturning circulation in eddying ocean models? *J. Phys. Oceanogr.*, **40**, 1520–1538, https://doi.org/10.1175/2010JPO4393.1.

Wunsch, C., 2002: What is the thermohaline circulation? *Science*, **298**, 1179–1181, https://doi.org/10.1126/science.1079329.

——, 2006: *Discrete Inverse and State Estimation Problems: With Geophysical Fluid Applications*. Cambridge University Press, 371 pp.

——, 2011: The decadal mean ocean circulation and Sverdrup balance. *J. Mar. Res.*, **69**, 417–434, https://doi.org/10.1357/002224011798765303.

——, and D. Stammer, 1995: The global frequency-wavenumber spectrum of oceanic variability estimated from TOPEX/

POSEIDON altimetric measurements. *J. Geophys. Res.*, **100**, 24 895–24 910, https://doi.org/10.1029/95jc01783.

——, and P. Heimbach, 2007: Practical global oceanic state estimation. *Physica D*, **230**, 197–208, https://doi.org/10.1016/j.physd.2006.09.040.

Wyrtki, K., 1962: The oxygen minima in relation to ocean circulation. *Deep-Sea Res. Oceanogr. Abstr.*, **9**, 11–23, https://doi.org/10.1016/0011-7471(62)90243-7.

Xu, Y. S., and L.-L. Fu, 2012: The effects of altimeter instrument noise on the estimation of the wavenumber spectrum of sea surface height. *J. Phys. Oceanogr.*, **42**, 2229–2233, https://doi.org/10.1175/JPO-D-12-0106.1.

Yang, X. Q., and E. Tziperman, 2022: Mid-depth ocean stratification: Southern Ocean eddies vs. interior vertical diffusivity. arXiv, 2105.15153v4, https://doi.org/10.48550/arXiv.2105.15153.